Polarization-based vision through haze

Yoav Y. Schechner, Srinivasa G. Narasimhan, and Shree K. Nayar

We present an approach for easily removing the effects of haze from passively acquired images. Our approach is based on the fact that usually the natural illuminating light scattered by atmospheric particles (airlight) is partially polarized. Optical filtering alone cannot remove the haze effects, except in restricted situations. Our method, however, stems from physics-based analysis that works under a wide range of atmospheric and viewing conditions, even if the polarization is low. The approach does not rely on specific scattering models such as Rayleigh scattering and does not rely on the knowledge of illumination directions. It can be used with as few as two images taken through a polarizer at different orientations. As a byproduct, the method yields a range map of the scene, which enables scene rendering as if imaged from different viewpoints. It also yields information about the atmospheric particles. We present experimental results of complete dehazing of outdoor scenes, in far-from-ideal conditions for polarization filtering. We obtain a great improvement of scene contrast and correction of color. © 2003 Optical Society of America

OCIS codes: 290.1310, 330.0330, 260.5430, 100.2000, 100.3020, 150.5670.

1. Introduction

Recently there has been a growing interest in the analysis of images acquired in poor-visibility conditions. The main objective has been to enhance[1–4] images taken in poor visibility and even restore clear-day visibility of the scene.[5–7] Some methods are based on specialized radiation sources and detection hardware.[8,9] For natural light, visibility degradation effects due to haze vary as distances to the objects increase,[10,11] and are referred to as aerial perspective.[12] For this reason, some image-enhancement methods proposed in the past require prior information about the distances of objects[3,4] or about the scene colors.[4]

It has been observed that aerial perspective can actually be exploited to obtain an estimated range map[6,7,13] of the scene. Computer vision methods have restored clear-day visibility of scenes using neither special radiation sources nor exact external knowledge about the scene structure or aerosols.[5,7] These methods relied only on the acquired images but required weather conditions to change between image acquisitions. This can take too long to make dehazing practical. In this paper we describe an approach that does not need the weather conditions to change and can thus be applied instantly.

Our approach is based on analyzing images taken through a polarizer. Polarization filtering has long been used in photography through haze.[14] Relying only on optical filtering is, however, restrictive: It is sufficient only on clear days, with weak light scattering (mainly due to air molecules), when the Sun is $\approx 90°$ to the viewing direction.[14,15] In these situations photographers have set the polarization filter at an orientation that best improves image contrast. In general, however, polarization filtering alone *cannot* remove the haze from images. Our method further analyzes optically filtered images to obtain significantly better results.

The effects of scattering on light polarization have been extensively studied.[16–21] Polarization has mainly been considered in the context of artificial illumination,[22–26] where the signal to be recovered is associated with polarized light while the light scattered by the medium is associated with depolarized light.[22–27] It has also been observed that an object masked by scattered light is enhanced by a linear superposition of polarization-filtered images.[28] In contrast we show that in hazy conditions, polarization can be associated with scattering of ambient illumination, rather than the signal (object radiance). Solving inverse problems associated with polarization-filtered images has proved to be useful in other regimes of scene analysis. For example, it

The authors are with Columbia Automated Vision Environment, Department of Computer Science, Columbia University, New York, New York 10027. Y. Schechner's e-mail address is yoav@cs.columbia.edu.

Received 18 January 2002; revised manuscript received 8 April 2002.

0003-6935/03/030511-15$15.00/0

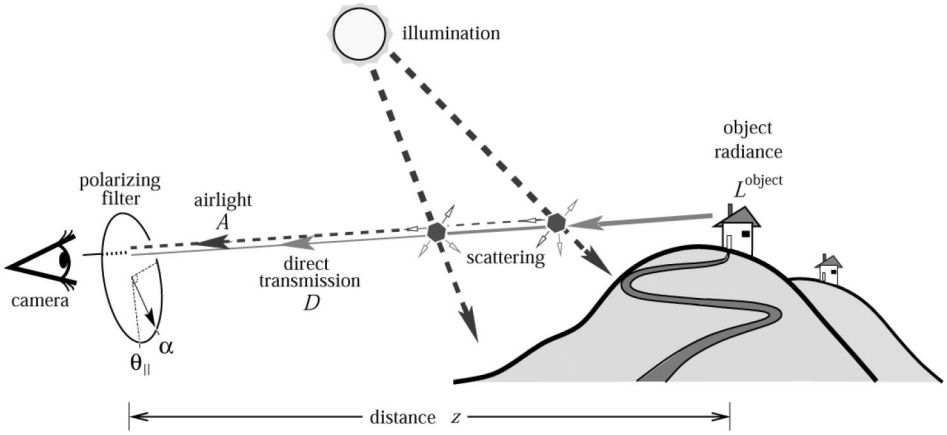

Fig. 1. (Dashed rays) Light coming from the illuminant (e.g., Sun) and scattered toward the camera by atmospheric particles is the airlight (path radiance) A. The airlight increases with the distance z of the object. (Solid ray) The light emanating from the object is attenuated along the line of sight as z increases, leading to the direct transmission D. Without scattering, object radiance would have been L^{object}. The scene is imaged through a polarizing filter at angle α. The polarization component parallel to the plane of incidence is best transmitted through the filter at $\alpha = \theta_{\|}$.

was used to separate transparent and semireflected scenes,[29,30] analyze specularities,[31–33] and classify materials.[34]

In this paper we describe an image-formation model that accounts for natural polarization effects in imaging through haze. We then invert the image-formation model to recover the dehazed scene and also to obtain information about scene structure and atmospheric properties. Our approach *does not* require modeling of the scattering particles' size or their precise scattering mechanisms. The principle is simple: The image is composed of two unknown components—the scene radiance in the absence of haze, and airlight (the natural illumination scattered toward the viewer). To recover these two unknowns, we need two independent images. We easily obtain these images because airlight is usually partially polarized. The method requires only that the airlight induce *detectable* partial polarization. We demonstrate removal of haze effects from real scenes in situations in which pure optical filtering (without applying our algorithm) does *not* suffice at all.

2. Theoretical Background

As depicted in Fig. 1, when imaging through the atmosphere we sense two sources. The first source is the scene object whose radiance is attenuated by scattering. The corresponding signal reaching the camera is called the *direct transmission*. The second source is the ambient illumination (Sun, sky, and so on). The part of the illumination scattered toward the camera by aerosols is called the *airlight*.[7,10,11,35,36] It is also referred to in the literature as path radiance[10] and veiling light.[37] In this section we describe each of these signals and the polarization effects associated with them.

A. Airlight Polarization

One of the causes of image degradation associated with atmospheric scattering is airlight. The atmosphere scatters light coming from the illumination sources (e.g., the Sun) toward the viewer[7] (see Fig. 1). The airlight increases with the distance z from the object. As discussed in Subappendix A.2,

$$A = A_{\infty}[1 - t(z)], \tag{1}$$

where A_{∞} is the airlight radiance corresponding to an object at an infinite distance, e.g., the horizon. $t(z)$ is the transmittance of incoherent light,[35] given by

$$t(z) = \exp\left[-\int_0^z \beta(z')\mathrm{d}z'\right], \tag{2}$$

where β is the coefficient of extinction due to scattering and absorption (see Subappendix A.2). When the extinction coefficient is distance invariant, $\beta(z') = \beta$, then

$$t(z) = \exp(-\beta z). \tag{3}$$

Assume for a moment that the illumination of any scattering particle comes from one direction (one illumination source). The light ray from the source to a scatterer and the line of sight from the camera to the scatterer define a plane of incidence. We divide the airlight into two polarization components that are *parallel* and *perpendicular* to this plane, $A^{\|}$ and $A^{\perp}$, respectively. The airlight degree of polarization is then

$$p \equiv (A^{\perp} - A^{\|})/A, \tag{4}$$

where

$$A = A^{\perp} + A^{\|} \tag{5}$$

is the total radiance due to airlight, given in Eq. (1).

The degree of polarization greatly varies as a func-

tion of the viewing and illumination directions, the density of the scattering particles, and their sizes. Depending on the size distribution of the scattering particles,[17,18,38] the airlight is partially linearly polarized either perpendicular to the plane of incidence[15,39] or parallel to it. When scattering is dominated by independent air molecules and small dust particles (Rayleigh scattering), $A^{\perp} \geq A^{\parallel}$. On the other hand, larger haze particles may cause $A^{\perp} < A^{\parallel}$. We use the following convention throughout this paper: To avoid confusion without loss of generality, we associate the parallel component notation ($\parallel$) with the minimum measured radiance at a pixel and perpendicular component notation ($\perp$) with the maximum radiance. We now explain the effectiveness of polarization in various haze and illumination conditions.

1. Trivial Case

Under special conditions, optical filtering alone is sufficient to remove haziness in images. For Rayleigh scattering,[14,15,34,36,40] the degree of polarization, p, is $(\sin^2 \phi)/(1 + \cos^2 \phi)$, where ϕ is the scattering angle (the angle between the illumination ray and the line of sight). Only when the light source is normal to the viewing direction is the airlight totally polarized ($p = 1$) perpendicular to the plane of incidence. Thus it can be eliminated if the image is captured through a polarizing filter oriented parallel to the plane of incidence. Dehazing in this case is trivial, since it is achieved with optical filtering alone. This situation is quite restricted, since it occurs only when the aerosols are very small and when the Sun is in a favorable position.

2. General Case

In general, the airlight will not be completely polarized.[36] Thus a polarizing filter cannot remove the airlight on its own. For example, in Rayleigh scattering the degree of polarization p decreases as the direction of illumination deviates from 90° (relative to the viewing direction). Reduction of polarization is caused by scattering from large haze particles, which never completely polarize light. Moreover, airlight due to large haze particles may be polarized orthogonally to light scattered by air molecules[17,18,38] causing partial annihilation of polarization. The degree of polarization p is also decreased by *depolarization*. This is caused by multiple scatterings from multiple directions: An illuminant of a scattering particle may be another particle in the air (e.g., a haze particle, a cloud drop, a molecule creating the skylight). Multiple scatterings[14,15,39,40] are more probable when the density of scatterers is high (poorer visibility). To make matters more complicated, these mechanisms depend on the wavelength.[14,15]

Fortunately, our algorithm *does not* require explicit modeling of the precise mechanisms of scattering. The method is based on the fact that even a partial polarization of the airlight can be exploited in postprocessing to remove scattering effects. This degree of polarization needs to be significant enough to be detected by the sensor. For this reason we concentrate in this paper on vision through haze, in which multiple scattering is much weaker than in fog. There are some weather conditions under which the algorithm may not be effective, as discussed in Section 8.

B. Direct Transmission Polarization

In addition to the presence of airlight, the scattering medium degrades images by attenuating the light emanating from scene objects. Let the object radiance be L^{object} in the absence of haze (scattering) between the scene and the viewer. When haze is present, as a ray of light progresses toward the viewer (Fig. 1), part of its energy is scattered in other directions, and a small portion of it may be absorbed. Thus the radiance sensed by the viewer is an attenuated fraction of L^{object}, called the *direct transmission*.[7] As a function of the distance z the direct transmission is

$$D = L^{\text{object}} t(z), \tag{6}$$

where $t(z)$ is given in Eq. (2).

We make three approximations in this paper. First, we concentrate on the degradation due to the attenuation of the signal and due to the additive airlight. We do not deal with image blur. Second, we take single-scattering effects to be dominant over multiple-scattering effects, which cause image blur and reduce the degree of polarization along the line of sight. Finally, we assume that light emanating from scene objects has insignificant polarization.

It follows from the last assumption that the polarization of the direct transmission is insignificant. If the scattering particles have random orientations, then the directly transmitted light will not be polarized in any macroscopically preferable orientation. Hence the polarization state of the unscattered light does not change,[39,40] although the radiance is attenuated.

The last assumption is invalid for specular surfaces. Nevertheless, when a specular object is far enough, its direct transmission makes a negligible contribution to the measured polarization. The reason is that the direct transmission decreases [Eq. (6)] whereas airlight[10] increases [Eq. (1)] with distance. Thus airlight and its polarization dominate the measured light for distant objects. Hence the model becomes more accurate where it is needed most—for distant objects that are most affected by haze. This property is useful if we know the relative distances to the scene objects.

Recall that airlight is just the aggregation of light scattered by particles at various distances along the line of sight. Since the polarization of this light does not change along the line of sight[39,40] p [Eq. (4)] does not depend on the distance.

The observations regarding the polarization described in Subsections 2.A and 2.B are unaffected by the exact dependence of t on z. The dominance of airlight polarization means that the polarizing filter

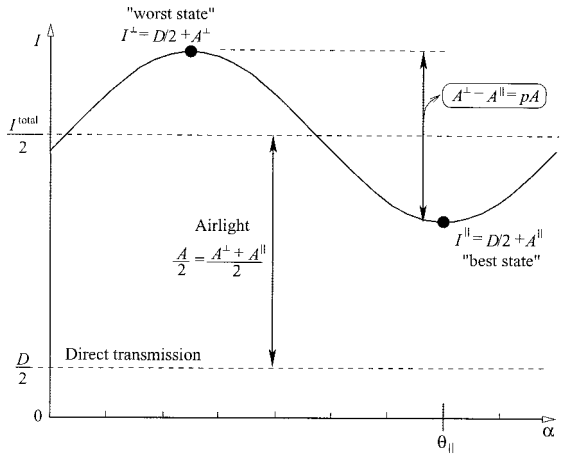

Fig. 2. At each point the minimum measured image irradiance as a function of α is $I^{\parallel}$. The maximum is $I^{\perp}$. The difference between these measurements is due to the difference between the airlight components $A^{\parallel}$, $A^{\perp}$. This difference is related to the unknown airlight A by the parameter p, which is the airlight degree of polarization. Without a polarizer the image irradiance is I^{total}, which is proportional to the sum of airlight and the unknown direct transmission.

modulates mainly the measured airlight but not the light originating from the objects. This is the key to subsequent calculations that remove the effects of haze.

3. Image Formation

The scene radiance is measured by the detector plane of the camera. The detected image irradiance is proportional to scene radiance. Since the proportionality depends on the optical system parameters and not on the weather effects, we treat the image irradiance and the scene radiance as equivalent. The overall radiance we sense is the incoherent sum of the airlight and the direct transmission. Without mounting a polarizer on the camera, the image irradiance is

$$I^{\text{total}} = D + A, \tag{7}$$

up to the said proportionality factor. It has been shown[10] that except for rather close objects (for which $\beta z < 0.2$), I^{total} is typically dominated by the airlight and not by the direct transmission. Thus typically most of the light we measure is not attributed to the signal D, whose origin is L^{object}. This is reinforced by the fact that most terrestrial objects have a low albedo, further decreasing the signal.

When a linear polarizer is mounted on the camera, the image irradiance changes as a function of the polarizer orientation angle α. Figure 2 describes the irradiance at a single pixel. The irradiance is a cosine function of α. On average, the image irradiance is $I^{\text{total}}/2$. (We do not deal here with the global absorptivity of unpolarized light that is common in sheet linear polarizers. Although this absorptivity effects the image irradiance, it does not modulate the effects of haze.)

One of our goals is to decouple the airlight and direct transmission. Since we assume that direct transmission is not polarized, its energy is evenly distributed between the polarization components. The variations due to the polarizer rotation are assumed to be mainly due to airlight. As seen in Fig. 2, when the polarizing filter is oriented such that the image irradiance is minimal ($\alpha = \theta_{\parallel}$), we measure

$$I^{\parallel} = D/2 + A^{\parallel}, \tag{8}$$

where [from Eqs. (4) and (5)]

$$A^{\parallel} = A(1 - p)/2. \tag{9}$$

This is the best state of the polarizer because here the image irradiance is the closest to the irradiance corresponding to the direct transmission (except for a factor of 1/2). There is a difference between $I^{\parallel}$ and $D/2$, because the airlight is not completely polarized ($A^{\parallel} \neq 0$).

In Section 4 we recover D by comparing two images taken with different orientations of the polarizer. For instance, one image can be $I^{\parallel}$, whereas the other,

$$I^{\perp} = D/2 + A^{\perp}, \tag{10}$$

is acquired when the filter is oriented perpendicular to $\theta_{\parallel}$. From Eqs. (4) and (5),

$$A^{\perp} = A(1 + p)/2. \tag{11}$$

From Eqs. (5), (8), and (10),

$$I^{\text{total}} = I^{\parallel} + I^{\perp}. \tag{12}$$

Note that $I^{\perp}$ is the worst state of the polarizer, because the airlight is enhanced relative to the direct transmission. To dehaze the image, we first have to remove the airlight A. The key step here is the estimation of p, the degree of polarization of airlight. As shown in Fig. 2, p relates the unknown airlight A to the difference between the image irradiances $I^{\perp}$ and $I^{\parallel}$.

Acquisition of polarimetric images is easy and feasible at the video rate.[34,41–44] However, for demonstration purposes we photographed the scene on a Fuji Sensia 100 slide film, using a common SLR (single-lens-reflex) (Cannon EOS-5) camera. The slides were scanned by a Nikon LS2000 35-mm film scanner. Before processing the images by the algorithm described in the following sections, we linearized the raw photographs to compensate for the system's radiometric response. This response was estimated from images of the Macbeth ColorChecker.[45] We modulated the polarization by mounting a standard linear polarizer on the camera lens.

We took images of a distant scene at two different orientations of a polarizer approximately corresponding to the perpendicular and the parallel airlight polarization components. The images are shown in Fig. 3. The raw images were *not* acquired in the trivial situation described in Subsection 2.A.1: The Sun was almost behind the camera (the Sun was in the south, and the picture was taken toward the north), whereas the haze was rather dense. For this

Fig. 3. Images of the polarization components corresponding to the minimal and the maximal radiances. Note that $I^{\parallel}$ (the image of irradiance) has the best image contrast that optics alone can yield, and yet there is no significant improvement over the image of the worst polarization state.

reason, $I^{\parallel}$ has only a slight improvement of image contrast relative to the contrast in $I^{\perp}$. Because of the partial polarization of the airlight, $I^{\parallel}$ was lower than $I^{\perp}$. For clarity of display, the brightness of each of the photos shown in Fig. 3 is contrast stretched.

4. Dehazing Images

Both the attenuation [Eq. (6)] and the airlight [Eq. (1)] depend on the distance z of the scene point. The distance to the objects is *spatially varying*, since different image pixels (x, y) correspond to objects at different distances. Therefore compensation for the effects of haze is spatially varying. Our dehazing method automatically accounts for this spatial variation of scene depth.

For each image pixel we have three unknowns: the object radiance (without haze) L^{object}, the airlight A, and the transmittance $t(z)$. These determine the irradiance at each image pixel. The airlight is related to $t(z)$ by Eq. (1). Thus the number of unknowns per pixel is reduced to two. These unknowns can be estimated from two images taken at almost any general unknown (but nondegenerate) orientations of the polarizing filter. We actually do not need the four measurements commonly used for full estimation of polarization. The reason for this is that the goal is not the estimation of polarization but the dehazing of the scene, and this can be done with two raw images. This is proved in Subappendix A.1. Nevertheless, the most-stable results are obtained if the algorithm is based on $I^{\parallel}$ and $I^{\perp}$. Therefore we focus here on this case.

Let the raw images correspond to the estimated polarization components, $\hat{I}^{\parallel}$ and $\hat{I}^{\perp}$. We assume that we have an estimate of the global parameters A_{∞} and p. Estimation of these parameters is described in Section 7. From Eqs. (8)–(11) it is seen that we can estimate the airlight of any point as

$$\hat{A} = (\hat{I}^{\perp} - \hat{I}^{\parallel})/p, \tag{13}$$

and the unpolarized image [Eq. (12)] as

$$\hat{I}^{\text{total}} = \hat{I}^{\parallel} + \hat{I}^{\perp}. \tag{14}$$

With Eq. (7) the estimated direct transmission is therefore

$$\hat{D} = \hat{I}^{\text{total}} - \hat{A}. \tag{15}$$

In this image the additive effect of the airlight is removed.

Recall that besides the addition of airlight, the haze attenuates the light coming from the object. The transmittance is estimated from Eqs. (1) and (13) as

$$\hat{t} = 1 - \hat{A}/A_\infty. \tag{16}$$

Thus we can compensate for the attenuation of the transmitted light. From Eqs. (6), (15), and (16) we obtain an estimate for the radiance that would have been sensed in the absence of atmospheric attenuation,

$$\hat{L}^{\text{object}} = \frac{\hat{I}^{\text{total}} - \hat{A}}{\hat{t}} = \frac{\hat{I}^{\text{total}} - \hat{A}}{1 - \hat{A}/A_\infty}. \tag{17}$$

$\hat{L}^{\text{object}}$ is hence the dehazed image. Dehazing thus amounts to simple pointwise operations such as subtraction and division of corresponding pixel values. Since different image pixels are processed independently, the spatially varying inversion of the haze effects is implicit: $\hat{A}$ is spatially varying, since it is larger for the more-distant objects.

We note that A_∞, p, and the extinction coefficient β are functions of the light wavelength λ. For Rayleigh scattering,[39,40] $\beta \sim 1/\lambda^4$, so the airlight in moderate haze is typically bluish. To account for the wavelength dependence, it is best to analyze the images with high spectral resolution. Each wavelength band can be analyzed independently. In our experiments, though, we used the traditional coarse wideband red, green, and blue (RGB) sampling of the spectrum.

We applied the dehazing method to the images shown in Fig. 3, after estimating the parameters A_∞ and p on the basis of sky measurements (for the parameter estimation, see Section 7 and in particular the stabilizing approach in Subsection 7.C). The resulting dehazed image is shown in Fig. 4(a). The brightness of the displayed image has the same scale as was used for displaying the best-polarized image $I^{\parallel}$ in the bottom of Fig. 3. The contrast of features in the dehazed image is greatly improved relative to $I^{\parallel}$ and $I^{\perp}$. Note, for instance, the distant mountain ridge (especially on the left), which is not visible in the raw images. Moreover, the algorithm removed the blue color bias, which existed in the raw images. This enables distinguishing the different vegetation types by hue. Although most of the scene is dehazed, the sky recovery is noisy, and there is a residual haziness at the more distant objects. These artifacts are explained is Subsection 7.C.

As another example consider the images shown in Figs. 5(a) and 5(b). Here $\hat{I}^{\parallel}$ and $\hat{I}^{\perp}$ were calculated from images taken at several orientations of the polarizer, as is commonly done in polarimetric imaging.[29,31] This experiment was conducted in conditions far from the trivial case: The haze was dense (visibility of a few kilometers), and the contrast in the parallel component was only slightly better than in the perpendicular component (all displayed images are linearly contrast-stretched versions of the raw images). The dehazed image is shown in Fig. 5(c). We obtain a significant improvement of contrast and color: The green forest is visible in the distant scene, whereas in the raw images that area looks like grayish-blue noise. The colors of the red bricks and roofs of the distant buildings are also restored.

5. Range Map of the Scene

A. Range Estimation

As a byproduct of the dehazing process we get an estimate of the range (depth) map of the scene. The estimation exploits the dependence of the transmittance t on the distance z. Note that t is always a monotonically decreasing function of z, and thus Eq. (16) immediately indicates the distance ordering of objects in the scene. Assuming the extinction coefficient to be distance invariant, $t(z) = \exp(-\beta z)$. Then, from Eq. (16),

$$\widehat{\beta z} = -\ln[1 - \hat{A}(x, y)/A_\infty]. \tag{18}$$

Note that the distance z is estimated as a function of (x, y) up to a global scale factor, which is the unknown extinction coefficient β.

Recall that we get an independent estimated range map for each color channel: $\widehat{\beta_r z}$, $\widehat{\beta_g z}$, and $\widehat{\beta_b z}$, where the subscripts r, g, b denote the three color channels. These maps should differ only in their scale. This scale is set by the ratios of their scalar extinction coefficients, β_r, β_g, and β_b. We combine the range maps into a single, average one:

$$\overline{\beta z}(x, y) \equiv [\widehat{\beta_r z}(x, y) + \widehat{\beta_g z}(x, y) + \widehat{\beta_b z}(x, y)]/3. \tag{19}$$

Note that there may be more optimal methods of combinations, such as a weighted average, in which the weights depend on the noise in each channel. The estimation may be further improved if it is based on narrow spectral bands, rather than on RGB.

We derived the range map of the scene corresponding to Fig. 3 as a byproduct of dehazing. To make the depth map more robust to noise, we median filtered $\hat{A}$. The range map is shown in Fig. 6. The darker points correspond to more distant objects. The map is qualitatively consistent with the scene, for example, indicating the close tree in the foreground and the gradual increase of range in the background.

The range map can be used to render the scene from viewpoints other than the one used during acquisition. We texture map the dehazed image on the range map (surface) and then look at the texture-

Fig. 4. (a) The dehazed image has much better contrast and color than the optically filtered image, especially in the distant regions of the scene (compare with Fig. 3). (b) and (c), As described in Section 5, we estimate the range map of the scene. We use it to render the dehazed scene from different perspectives, as if the viewer descends. Note the occlusion of the background by the foreground tree on the right. Note also the distant mountains occluded by the closer ridge.

mapped surface from various viewpoints. Examples for this application are shown in Figs. 4(b) and 4(c). Here the appearance of the scene is shown from two different viewpoints. The images are rendered by rotation of the textured surface by 22° and 31° relative to normal viewing direction shown at the top of Fig. 4. This creates the impression that the viewer gradually descends relative to the acquisition position.

One may see that the valley with the agricultural segments is planar, since straight lines on it remain quite straight when viewed from different directions. It can clearly be seen in Fig. 4 how the large tree on the right-hand side of foreground occludes the buildings in the valley behind it and the mountain range bounding the valley. In addition, one may see that there are consecutive mountain ranges (the close one, which bounds the valley, is greener, whereas the farther ones are more pale as explained in Subsection 7.C). As the viewer descends, the farther ridges become occluded by the close ridge, and as the viewer ascends, the distant ridges gradually appear.

B. Range Accuracy

We now analyze the accuracy of range estimation on the basis of scattering. Let the uncertainty (scaled by the camera's dynamic range) in the measurement of $\hat{I}^{\parallel}$ or $\hat{I}^{\perp}$ be $\sigma = 2^{-b}$. Here b is the number of bits per pixel of the camera, assuming that quantization is the dominant noise source and that the radiometric response is linear. The uncertainty of the estimated depth is then

$$\delta z \approx \frac{1}{\beta} \exp(\beta z - b \ln 2) \frac{1}{pA_{\infty}}. \tag{20}$$

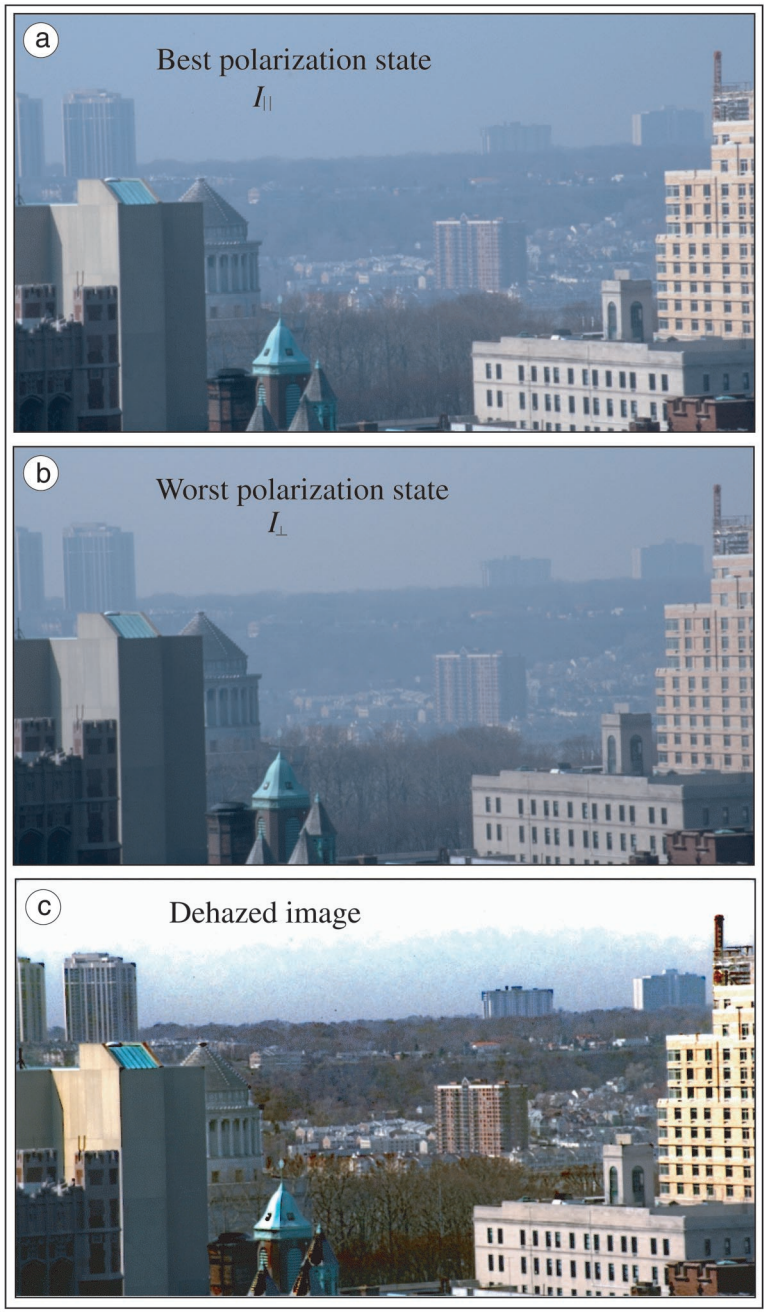

Fig. 5. Photograph with the best contrast that optics alone can give (a) is almost as poor as the worst polarization state (b). The dehazed image (c) has much better contrast and color, especially in the distant regions of the scene (note the green forest and the red roofs).

The range uncertainty grows exponentially with the distance. Beyond some distance $z_{\max}$, range estimation is too uncertain to be reliably considered. Nevertheless, relation (20) shows that the degrading effect due to growth of distance z can be compensated by a proportional increase of the number of bits b. Thus, $z_{\max} \propto b$. For example, a 12-bit camera will be able to probe 50% farther into the scene than an 8-bit camera.

One may note that haze can actually be useful for estimating distances, since without scattering the perception of depth due to airlight is lost. Indeed, $\delta z \to \infty$ when $\beta \to 0$, i.e., when attenuation is weak. On the other hand, $\delta z \to \infty$ also when $\beta \to \infty$, that is, when attenuation is too strong (e.g., in fog). The optimal extinction coefficient minimizing δz is $\beta = 1/z$. For example, estimates of object ranges around the distance of 3 km are most accurate on a day when the effective attenuation distance due to haze is 3 km [$\beta = 1/3$ (km^{-1})].

The estimation is prone to significant error for close objects reflecting significantly polarized light such as specular objects. As discussed in Subsection 2.B, the degree of polarization of the distant, hazy objects is small relative to the airlight. This may not be true for close objects. Figure 7 shows

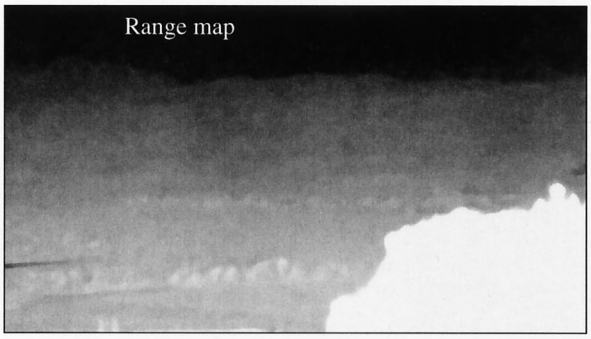

Fig. 6. Range map of the scene shown in Fig. 3, estimated as a byproduct of the dehazing algorithm. The farther the object, the darker the shading.

the range map obtained for the scene shown in Fig. 5. The map is qualitatively consistent with the scene, for instance, indicating the close buildings and the distant ridge. Yet a significant partial polarization was observed in some surfaces on the close buildings, especially those directly lit by the Sun. In Fig. 7 this manifests in a dark shading of the points corresponding to these objects (rather than a bright shade). Note also that haze homogeneity is the basis for Eq. (18); thus range estimation becomes less accurate when there are significant spatial variations of the haze.

To conclude this section, using haze and polarization to estimate a range map of the scene is prone to several sources of inaccuracy. Nevertheless, it enables passive estimation of very long distances, without resorting to geometric methods (triangulation), which are prone to matching problems. Instead of geometry, the use of photometry enables the rough estimation of the large distances from a single viewpoint. The limit of the estimated range depends on the visibility. We demonstrated ranging in a scene with visible objects tens of kilometers away, but the maximum range can be much larger, depending on β and b.

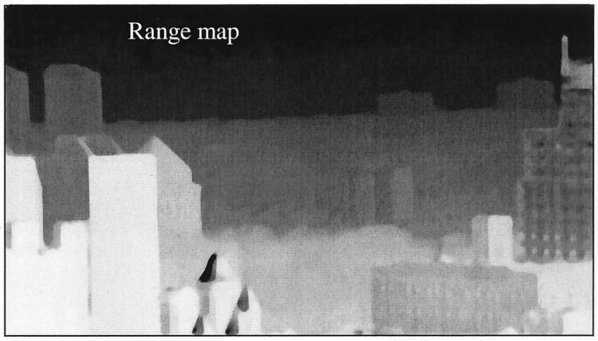

Fig. 7. Range map of the scene shown in Fig. 5, estimated as a byproduct of the dehazing algorithm. Some surfaces of close objects are wrongly marked as distant ones as a result of their high degree of polarization.

6. Information about the Aerosols

In Section 4 we showed that on the basis of as few as two images we can dehaze the imaged scene. Now we will show that with the same raw images we can extract information related to the atmospheric particles that degrade the scene visibility.

Consider the range maps of each color channel, which were described in Section 5. Averaging over the image pixels, we define scalars corresponding to each color channel:

$$s_r = \frac{\sum_{x,y} \widehat{\beta_r z}(x, y)}{\sum_{x,y} \overline{\beta z}(x, y)}, \tag{21}$$

$$s_g = \frac{\sum_{x,y} \widehat{\beta_g z}(x, y)}{\sum_{x,y} \overline{\beta z}(x, y)}, \tag{22}$$

$$s_b = \frac{\sum_{x,y} \widehat{\beta_b z}(x, y)}{\sum_{x,y} \overline{\beta z}(x, y)}. \tag{23}$$

These scalars express the extinction coefficients of the atmosphere, in each of the color channels, up to a single scale factor. This result is valuable because the relative scattering coefficients are determined by the size of the scattering particles.[2,15,39] Assuming that scattering is the dominant process of attenuation, these ratios provide rough indication about the distribution of the particles' size. This information may be used in conjunction with other methods for estimating the particle size from spectral and polarization information.[16] It may be incorporated into models that make explicit physical analysis of atmospheric scattering, as well as in applications of ecological monitoring. As with image dehazing and range estimation, this application would be more accurate if narrow spectral bands were used, rather than RGB.

In the experiment based on the images shown in Fig. 5, we obtained

$$\begin{pmatrix} s_r \\ s_g \\ s_b \end{pmatrix} = \begin{pmatrix} 0.26 \\ 0.32 \\ 0.42 \end{pmatrix}, \tag{24}$$

which means that the scattering in the blue band is $\sim$60% stronger than the scattering in the red band. Had the dominant particles been small enough to obey Rayleigh's $1/\lambda^4$ rule, we might have expected that the scattering of the blue wavelengths were much stronger relative to the red wavelengths. It is difficult to pinpoint the exact relative strength when very broadband spectral channels are used. So to get a rough estimate, if we take 450 and 650 nm as typical mid-band wavelengths for blue and red, respectively, then in Rayleigh scattering we may expect the blue scattering to be (an order of) 300% stronger

than the red one. Therefore, as expected, the experiment was conducted under conditions in which scattering was dominated by particles that do not fit into the Rayleigh model. Therefore, even if the Sun had been perpendicular to the viewing direction (the trivial case for Rayleigh scattering), light would not have been sufficiently polarized to enable dehazing by optical filtering alone.

7. Estimating A_∞ and p

To dehaze the image with Eqs. (13), (15), and (17), we need an estimate of the global parameters A_∞ and p. In Ref. 10 it was concluded that human vision can correct for effects of aerial perspective on the basis of context. We use this observation as the way to obtain A_∞ and p. The image context we mainly rely on is the sky. This section discusses estimation of these parameters. The experimental results were based on the principles described in Subsections 7.A–7.C.

A. Sky Measurements at the Horizon

Since $t(z) \to 0$ as $z \to \infty$, we get

$$I^{\text{total}} = L^{\text{object}} t(z) + A_\infty [1 - t(z)] \to A_\infty. \qquad (25)$$

The degree of polarization of the measured scene (i.e., the direct transmission combined with airlight) is

$$\hat{P}(x, y) = \frac{\Delta I(x, y)}{I^{\text{total}}(x, y)}, \qquad (26)$$

where

$$\Delta I(x, y) \equiv [\hat{I}^{\perp}(x, y) - \hat{I}^{\parallel}(x, y)]. \qquad (27)$$

As $z \to \infty$,

$$\hat{P}(x, y) \to \frac{A_\infty{}^{\perp} - A_\infty{}^{\parallel}}{A_\infty{}^{\perp} + A_\infty{}^{\parallel}} = p. \qquad (28)$$

We can measure these parameters directly from the images. We can use points that are seen through enough haze such that their direct transmission is practically zero. Such points are not always available, so we use some heuristics based on context (as in human vision[10]) to estimate these parameters. The most direct way is to measure patches of the sky at the horizon:

$$\hat{A}_\infty = I^{\text{total}}(\text{sky}), \qquad \hat{p} = \frac{\Delta I(\text{sky})}{I^{\text{total}}(\text{sky})}. \qquad (29)$$

As an example, in the experiment corresponding to the images shown in Fig. 5, the average measured values of $\hat{p}$ with Eq. (29) were

$$\begin{pmatrix} \hat{p}_r \\ \hat{p}_g \\ \hat{p}_b \end{pmatrix} \approx \begin{pmatrix} 0.28 \\ 0.25 \\ 0.22 \end{pmatrix}. \qquad (30)$$

Note that $\hat{p}_r > \hat{p}_g > \hat{p}_b$. This is consistent with the literature[14,15]: In haze, long wavelengths (red) undergo less multiple scattering and therefore maintain a higher degree of polarization, compared with short (blue) wavelengths. Since p depends on the size and density of the scatterers,[15] the estimation of p in the different spectral bands may provide additional information about the aerosols in the scene.[16]

Note that if the horizon is cloudy and $t(\infty) \neq 0$, then the measured light is due not only to haze airlight but also to the object (cloud). Thus this method will be erroneous, and we may need to apply the method described in Subsection 7.D.

B. Spatial Variability

Although we treat the parameters A_∞ and p as global, they may vary across the field of view. The sky (horizon) radiance A_∞ depends on the angular scattering coefficient $\beta(\phi)$, as explained in Subappendix A.2. Therefore it depends on the position of the Sun relative to the viewing direction.[12] For instance, because of strong forward scattering and backscattering, A_∞ will usually be larger when the Sun is in front or behind the camera. Also, p depends on the position of the Sun relative to the viewing direction.

The spatial variations of A_∞ and p across the field of view are much slower than the typical variations in radiance that are due to texture. Thus we can account for the horizontal variation of A_∞ and p by sparsely sampling the sky radiance at the horizon across the field of view and then interpolating the values, using a smoothly varying function. In the experiments we performed we estimated $\hat{A}_\infty$ and $\hat{p}$ by sparsely measuring the sky values above the distant ridges across the images. We then fit a second-order polynomial to the measurements.

Vertical variations are more complicated. Sky measurements can change as a function of altitude. Haze density can change significantly as a function of altitude[11] within the first few vertical kilometers of atmosphere,[2] and even within a few hundred meters. Moreover, even on a clear day the sky radiance and polarization change as a function of the viewing direction relative to the zenith.[38,46] The plane of polarization may change by 90° above the solar and antisolar horizons when the Sun is low. Thus one has to be careful when applying this method in a large vertical field of view. A direct implication is that measuring $\hat{A}_\infty$ and $\hat{p}$ from a sky patch at high elevation angle will usually be error prone. For this reason we measure the sky values close to the horizon. We also applied a stabilizing bias, described next.

C. Stabilizing the Recovery

Even if all the measurements were perfect, we believe that avoiding a complete inversion of the image formation is beneficial from a perceptual-aesthetic point of view. There are two reasons for this. First, attempting to remove the atmospheric scattering from the sky itself means that the daylight sky should be removed. In a noiseless image the result would be dark deep-space sky in a clear daylight image! This is perceptually annoying. The sky appearance is further degraded by unstable amplification of noise,

since the denominator in Eq. (17) approaches zero when $\hat{A} \to A_\infty$. Second, even on the clearest day, we still encounter airlight because of scattering by the air molecules, which manifests in a bluish tint in the distance. Images lacking any aerial perspective,[12] in which far objects are the same as close ones, look strange and artificial.

If the dehazed images are meant for human inspection, it is preferable to avoid these phenomena. This is easily achieved if we somewhat bias $\hat{p}$ by multiplying it by a factor ϵ, such that $1 \le \epsilon \le 1/\hat{p}$:

$$\hat{p} \to \epsilon\hat{p}. \tag{31}$$

If $\epsilon = 1$, we get Eq. (17) as the solution to the inverse problem. In the other extreme we may set $\epsilon\hat{p} = 1$ (recall that $p \le 1$), and then the algorithm behaves as if the airlight were completely polarized: From Eqs. (13) and (15) $D(x, y) = \hat{I}^{\parallel}(x, y)$ when $p = 1$; hence the unprocessed best-polarized image component is used as the value for the direct transmission. For all intermediate values of ϵ the inverse solution (17) is moderated by means of weighting it with the raw image. Using a value of ϵ slightly larger than 1 leaves a residual haziness (originating from the raw image) that grows with the distance, thus making the image consistent with naked-eye experience. It can also be shown that when $\epsilon > 1$ the estimated dehazed sky value is $\hat{L}^{\text{object}}(\text{sky}) = A_\infty$; i.e., it retains its raw unpolarized sky value, automatically. The noise in the estimated sky value is

$$\delta\hat{L}^{\text{object}}(\text{sky}) = \sqrt{2}\sigma(1 - 1/\epsilon)^{-1}, \tag{32}$$

where σ is the noise standard deviation of the raw image components. It can be seen that noise is amplified in the sky by the dehazing process, but this amplification decreases with the increase of ϵ.

This bias is also beneficial to counter effects of error stemming from inaccurate estimation of p and A_∞. As described in Subsection 7.B, we may expect such inaccuracy if it is based on sky measurements. From Eqs. (13)–(15), (26), and (27),

$$\hat{D}(x, y) = \frac{\hat{I}^{\text{total}}(x, y)}{\hat{p}}\,[\hat{p} - \hat{P}(x, y)]. \tag{33}$$

If our estimate of the airlight degree of polarization is too low ($\hat{p} < p$), then negative values can appear in the image of the direct transmission. This is especially relevant to distant objects, because $P(x, y) \to p$ when $z \to \infty$. Biasing $\hat{p}$ with Eq. (31) reduces the occurrence of such problems. In addition, Eq. (31) better conditions the compensation for attenuation in case $\hat{A}_\infty$ is inaccurate [see Eqs. (13), (16), and (17)].

In the experiments we performed, we first estimated $\hat{A}_\infty$ and $\hat{p}$ as described in Subsections 7.A and 7.B. Indeed, that heuristic method resulted in a slight error, and many of the resulting pixels of $\hat{D}$ and $\hat{L}^{\text{object}}$ had negative values, especially in the distant areas. In addition, the sky was quite noisy. So, to get the dehazing results presented in this paper, we fine tuned $\hat{p}$ by increasing its values globally by a few percent ($\epsilon = 1.09$). We thus gave up a few percent of the full inversion, and in return almost all the occurrences of negative values were eliminated and the sky regained a natural color (a tolerable noise is still present). As can be seen in Fig. 4, distant objects have a residual bluish haziness (aerial perspective[12]), making the recovered scene look perceptually acceptable.

D. Unavailable Sky Measurements

When direct sky measurements are not possible to obtain, we need to get the context for estimating p and A_∞ from nonsky regions of the scene. We now show that such an estimate can be obtained from *a priori* information about the identity of several scene points with similar but unknown radiance L^{object}, had the haze been absent. For instance, this is possible if parts of the scene had been observed on a clear day so that some objects are known to have corresponding colors. From Eqs. (13), (17), and (27),

$$\hat{I}^{\text{total}}(x, y) = L^{\text{object}} + \left(\frac{1}{p} - \frac{L^{\text{object}}}{pA_\infty}\right)\Delta I(x, y). \tag{34}$$

Assume that we know of a set of (at least two) pixels (x_k, y_k) for which the object radiance in the absence of haze is the same, $L^{\text{object}} = {L_1}^{\text{object}}$, but their distances from the viewer are different. For instance, the set of pixels can correspond to similar bushes at different distances. The value ${L_1}^{\text{object}}$ does not have to be known in advance, as we will see in the following. Because of the differing depths, these points (x_k, y_k) will have different values of $\hat{I}^{\text{total}}(k)$ and $\Delta I(k)$. For all these points, however,

$$C_1 \equiv \left(\frac{1}{p} - \frac{{L_1}^{\text{object}}}{pA_\infty}\right) \tag{35}$$

is constant. Thus $\hat{I}^{\text{total}}(k)$ as a function of $\Delta I(k)$ forms a straight line,

$$\hat{I}^{\text{total}}(k) = {L_1}^{\text{object}} + C_1\Delta I(k), \tag{36}$$

whose intercept on the $\hat{I}^{\text{total}}$ axis is the radiance value ${L_1}^{\text{object}}$. Therefore knowing points (x_k, y_k) that have corresponding radiances, we can estimate their corresponding dehazed radiance by fitting a line to the measured $\hat{I}^{\text{total}}(k)$ and $\Delta I(k)$. The slope of the fitted line is C_1.

Now that we know ${L_1}^{\text{object}}$ and C_1, we may rewrite Eq. (35) as

$$p = \frac{1}{C_1} - (L_1^{\text{object}}/C_1)\,\frac{1}{A_\infty}. \tag{37}$$

Thus the unknown p and A_∞ are constrained to lie on a line in the $(p, 1/A_\infty)$ plane. The line is defined by the already estimated L_1^{object} and C_1. Now we can look at a different set of (at least two) pixels (x_n, y_n), which in the absence of scattering effects have the same radiance L_2^{object}, where $L_2^{\text{object}} \ne L_1^{\text{object}}$. Once again, analogous to Eqs. (35) and (36), L_2^{object} and the corresponding C_2 are estimated if the pixels (x_n, y_n)

correspond to scene points at different distances. This supplies another line constraint,

$$p = \frac{1}{C_2} - (L_2^{\text{object}}/C_2)\,\frac{1}{A_\infty}. \tag{38}$$

The intersection of these lines (37, 38) yields the estimated values for p and A_∞. For $N > 2$ sets of pixels corresponding to unknown dehazed object radiances L_l^{object} where $l = 1, \ldots, N$, the estimation of p and A_∞ becomes more robust. The minimum, however, is two sets of two points. Note that for identifying the sets of pixels, this method requires some user interaction, as in the estimation using sky measurement.

8. Discussion

We have shown that physics-based image analysis that follows acquisition of polarization-filtered images can remove visual effects of haze. Although it is based on some approximations, this approach proved to be effective in dehazing, when the problem could not be solved by optics alone. The method is quick and does not require temporal changes in weather conditions. In addition to the dehazed image, the method also yields information about scene structure and the atmospheric particles. These results can form the basis for useful tools in photography and remote sensing.

Our method is based on the partial polarization of airlight. Therefore its stability will decrease as the airlight degree of polarization decreases. For instance, the method may be less effective when the illumination is less directional (overcast skies). We expect it to have just a limited effect, or even fail, in cases of strong depolarization, as occurs in fog. Nevertheless, with more-exact scattering models, such as those that include multiple scattering, this research may be extended to complicated weather conditions and perhaps to other scattering media (e.g., underwater environments[34] and tissues).

Appendix A

1. Dehazing with Two Arbitrary Images

In Sections 4 and 5 we used estimates of $I^{\parallel}$ and $I^{\perp}$ in the dehazing algorithm. We now show that in theory the method can work on the basis of two images taken through any nondegenerate polarization orientations. Let $\theta_{\parallel}$ be the orientation of the polarizer for best transmission of the component parallel to the plane of incidence (Fig. 1). For a general orientation α the observed airlight is

$$A(\alpha) = A\{1 - p\,\cos[2(\alpha - \theta_{\parallel})]\}/2, \tag{A1}$$

which coincides with Eqs. (9) and (11) if $\alpha = \theta_{\parallel}$, $\theta_{\parallel} + 90°$. Assume that we take two images of the scene with arbitrary orientations of the polarizer, $\alpha_1 \neq \alpha_2$. Because the direct transmission is unaffected by the polarizer orientation, the images are

$$I_1 = D/2 + A(\alpha_1), \tag{A2}$$

$$I_2 = D/2 + A(\alpha_2). \tag{A3}$$

Let us define an effective airlight

$$A_{\text{effective}} \equiv A(\alpha_1) + A(\alpha_2), \tag{A4}$$

with an effective degree of polarization

$$p_{\text{effective}} \equiv \frac{A(\alpha_2) - A(\alpha_1)}{A_{\text{effective}}}, \tag{A5}$$

where we set $A(\alpha_2) \geq A(\alpha_1)$, without loss of generality. We also define an effective unfiltered image

$$I_{\text{effective}}^{\text{total}} \equiv I_1 + I_2 = D + A_{\text{effective}}. \tag{A6}$$

It can easily be shown that $A_{\text{effective}}$ is proportional to the actual airlight,

$$A_{\text{effective}} = fA = fA_\infty[1 - t(z)] = A_\infty^{\text{effective}}[1 - t(z)], \tag{A7}$$

where $A_\infty^{\text{effective}}$ is the effective airlight at infinity (the horizon). The proportion factor f is

$$f = 1 - p\,\cos(\alpha_1 + \alpha_2 - 2\theta_{\parallel})\cos(\alpha_1 - \alpha_2). \tag{A8}$$

Since we do not know $\theta_{\parallel}$ on the basis of two arbitrary polarizer angles, f is unknown.

Assume now that we have estimates of the parameters $p_{\text{effective}}$ and $A_\infty^{\text{effective}}$. These parameters can be estimated by measurement of the image irradiances I_1 and I_2 at the sky, similar to the way described in Section 7. Then we estimate the effective airlight at each point,

$$\hat{A}_{\text{effective}} = \frac{I_2 - I_1}{p_{\text{effective}}}. \tag{A9}$$

From Eq. (A6) the estimated direct transmission based on the raw images I_1 and I_2 is

$$\hat{D} = I_{\text{effective}}^{\text{total}} - \hat{A}_{\text{effective}}. \tag{A10}$$

From Eq. (A7) the estimated transmittance is

$$\hat{t} = 1 - \frac{\hat{A}_{\text{effective}}}{A_\infty^{\text{effective}}}. \tag{A11}$$

Thus the dehazed image is

$$\hat{L}^{\text{object}} = \frac{I_{\text{effective}}^{\text{total}} - \hat{A}_{\text{effective}}}{1 - \hat{A}_{\text{effective}}/A_\infty^{\text{effective}}}. \tag{A12}$$

We can check the stability of using an arbitrary pair of images. It is easy to show that

$$p_{\text{effective}} = \frac{Ap}{A_{\text{effective}}}\,\sin(\alpha_1 + \alpha_2 - 2\theta_{\parallel})\sin(\alpha_2 - \alpha_1). \tag{A13}$$

Equation (A9) becomes unstable when $p_{\text{effective}} \to 0$. Besides the obvious case in which $p = 0$, this happens when

$$(\alpha_1 + \alpha_2)/2 = \theta_{\|},\ \theta_{\|} + 90^\circ. \tag{A14}$$

This is expected because the acquired images are equal if taken on symmetric angles relative to the extrema of the cosine in Eq. (A1). Therefore changing the orientation from α_1 to α_2 is degenerate. Except for these singular cases, dehazing is possible with two images. The best stability of dehazing is achieved when $p_{\text{effective}}$ is maximum, that is, when $\alpha = \theta_{\|},\ \theta_{\|} + 90^\circ$. Therefore we focus here on dehazing based on $I^{\|}$ and $I^{\perp}$.

By rotating the polarizer to achieve an extremum of the image irradiance or contrast, it is often easy to detect visually the states corresponding to $I^{\|}$ and $I^{\perp}$. However, it is easier and more accurate to estimate these components with 3 or more images taken through different general orientations of the polarizer. This is a common practice in polarization imaging, as detailed in Refs. 29, 31, 34, 43, 47, and 48.

2. Inhomogeneous Attenuation: Model and Recovery

This subsection describes the image-formation model and the dehazing method when the attenuation varies along the line of sight. It is given here mainly to make the paper self-contained for readers unfamiliar with radiative transfer. When light propagating toward the camera passes through an infinitesimal layer of scattering media, some percentage of it is lost as a result of scattering to other directions and as a result of absorption. For a layer of thickness $\mathrm{d}z'$, the direct transmission change $\mathrm{d}D$ is given[7,36] by the differential equation

$$\frac{\mathrm{d}D(z')}{D} = -\beta(z')\mathrm{d}z'. \tag{A15}$$

$\beta(z')$ is the extinction coefficient at depth z'. We obtain it by integrating the angular scattering coefficient $\beta(\phi, z')$ over all scattering angles ϕ and adding the absorption coefficient, if absorption exists. When we integrate Eq. (A15) over the distance z from the object, the measured transmitted light is $D = L^{\text{object}} t(z)$, where $L^{\text{object}} = D|_{z=0}$, and the atmospheric transmittance is

$$t(z) = \exp\left[-\int_0^z \beta(z')\mathrm{d}z' \right]. \tag{A16}$$

In the special case when $\beta(z') = \beta$ independently of the distance, we obtain Eq. (3).

Now let us derive the expression for airlight. Consider a layer of scattering media, of infinitesimal depth $\mathrm{d}z''$ illuminated by a light source at an arbitrary direction (say, the Sun). Part of this light is scattered *toward* the camera. The radiance of the scattered light is proportional to the angular scattering coefficient $\beta(\phi, z'')$. Note[7] that $\beta(\phi, z'') \propto \beta(z'')$. This is because light scattered toward a certain direction is a fraction of the total amount of light removed from the incident beam by scattering in all directions and by absorption. The scattered light radiance is also proportional to both the illumination irradiance and to $\mathrm{d}z''$. Thus we may conclude that the ambient light scattered by this layer toward the camera is given by $\kappa\beta(z'')\mathrm{d}z''$, where κ encapsulates the illumination irradiance and the proportion of light scattered in the direction of the camera, relative to the total scattering (and absorption). This expression also describes the case in which the layer is illuminated by a distribution of source directions.[7]

Once this light has been directed toward the camera, it undergoes attenuation on its way, as dictated by $t(z'')$. Eventually, the airlight from the above-mentioned layer is

$$\mathrm{d}A(z'') = \kappa\beta(z'')\mathrm{d}z'' \exp\left[-\int_0^{z''} \beta(z')\mathrm{d}z' \right]. \tag{A17}$$

The total airlight radiance (path radiance) is obtained by means of integrating the airlight contribution from all layers[49]:

$$\begin{aligned} A(z) &= \int_0^z \mathrm{d}A(z'') = -\kappa \left\{ \exp\left[-\int_0^{z''} \beta(z')\mathrm{d}z' \right] - 1 \right\}_0^z \\ &= \kappa[1 - t(z)]. \end{aligned} \tag{A18}$$

The airlight of a scene point at infinity is

$$A_\infty = \kappa[1 - t(\infty)]. \tag{A19}$$

Therefore the airlight is

$$A = \frac{A_\infty}{1 - t(\infty)}[1 - t(z)]. \tag{A20}$$

In the homogeneous haze model [Eq. (3)] we have $t(\infty) = 0$, that is, object points that are far enough are completely attenuated. If we apply the assumption of total attenuation for objects at infinity also to inhomogeneous haze, then we set $t(\infty) = 0$ in Eq. (A20). We then obtain

$$A = A_\infty[1 - t(z)], \tag{A21}$$

as in Eq. (1). This is the situation assumed throughout the paper.

It is interesting to examine how the solution is influenced when $t(\infty)$ is unknown and is not zero. Assume that we perform the recovery in the same way. First, we estimate $\hat{p}$ and $\hat{A}_\infty$ by sampling the image of the sky, as in Subsection 7.A. This time,

$$\Delta I(\text{sky}) = A_\infty p, \tag{A22}$$

while

$$I^{\text{total}}(\text{sky}) = L^{\text{object}}(\text{sky})t(\infty) + A_\infty. \tag{A23}$$

Fortunately, we can set $L^{\text{object}}(\text{sky}) = 0$. The reason for this is that at night, when there is no airlight ($A_\infty = 0$), the sky is dark [$I^{\text{total}}(\text{sky}) = 0$]. Therefore,

when airlight exists, $I^{\text{total}}(\text{sky}) = A_\infty$. Hence we can safely use Eqs. (29) to estimate $\hat{A}_\infty$ and $\hat{p}$.

Now that we have the parameters, we can look at the scene-dehazing equation. It can be shown that the estimation of the direct transmission $\hat{D}$ with Eq. (15) and $\hat{p}$ is correct. Therefore we can remove the additive airlight, using the same procedure as with $t(\infty) = 0$. To complete the dehazing process, we need to compensate for the attenuation. Similar to Eqs. (15) and (17),

$$\hat{L}^{\text{object}} = \hat{D}/\hat{t}. \tag{A24}$$

This time [see Eq. (A20)],

$$\hat{t} = 1 - \frac{\hat{A}}{A_\infty}[1 - t(\infty)], \tag{A25}$$

which is somewhat different from Eq. (16). If $t(\infty)$ is unknown and cannot be neglected, then our estimation of the transmittance with Eq. (16) is biased toward a value lower than the true one. This will lead to some overamplification (brightening) of the image radiance corresponding to distant objects in the dehazed image. The overamplification of distant objects is reduced when we bias $\hat{p}$ by a factor of $\epsilon > 1$ as in relation (31); this bias reduces $\hat{A}$, thereby increasing $\hat{t}$ in Eq. (16) in the same way as the factor $[1 - t(\infty)]$ does in Eq. (A25).

Partial and preliminary results were presented in Ref. 47. We thank the reviewers for their helpful remarks. This study was supported in part by a grant from the Defence Advance Research Projects Agency (DARPA) Human Identification at a Distance program, contract N00014-00-1-0916; by National Science Foundation (NSF) award IIS-99-87979; and by the Morin Foundation.

References and Note

1. L. Grewe and R. R. Brooks, "Atmospheric attenuation reduction through multi-sensor fusion," in *Sensor Fusion: Architectures, Algorithms, and Applications II*, B. V. Dasarathy, ed., Proc. SPIE **3376,** 102–109 (1998).
2. N. S. Kopeika, *A System Engineering Approach to Imaging* (SPIE, Bellingham, Wash., 1998), pp. 446–452.
3. J. P. Oakley and B. L. Satherley, "Improving image quality in poor visibility conditions using a physical model for contrast degradation," IEEE Trans. Imag. Proc. **7,** 167–179 (1998).
4. K. Tan and J. P. Oakley, "Physics-based approach to color image enhancement in poor visibility conditions," J. Opt. Soc. Am. A **18,** 2460–2467 (2001).
5. S. G. Narasimhan and S. K. Nayar, "Chromatic framework for vision in bad weather," in *Proceedings of the IEEE Conference on Computer Vision and Pattern Recognition* (Institute of Electrical and Electronics Engineers, New York, 2000), Vol. I, pp. 598–605.
6. S. G. Narasimhan and S. K. Nayar, "Removing weather effects from monochrome images," in *Proceedings of the IEEE Conference on Computer Vision and Pattern Recognition* (Institute of Electrical and Electronics Engineers, New York, 2001), Vol. II, pp. 186–193.
7. S. K. Nayar and S. G. Narasimhan, "Vision in bad weather," in *Proceedings of the IEEE International Conference on Computer Vision* (Institute of Electrical and Electronics Engineers, New York, 1999), pp. 820–827.
8. P. S. Pencikowski, "Low-cost vehicle-mounted enhanced vision system comprised of a laser illuminator and range-gated camera," in *Enhanced and Synthetic Vision*, J. G. Verly, ed., Proc. SPIE **2736,** 222–227 (1996).
9. B. T. Sweet and C. L. Tiana, "Image processing and fusion for landing guidance," in *Enhanced and Synthetic Vision*, J. G. Verly, ed., Proc. SPIE **2736,** 84–95 (1996).
10. R. C. Henry, S. Mahadev, S. Urquijo, and D. Chitwood, "Color perception through atmospheric haze," J. Opt. Soc. Am. A **17,** 831–835 (2000).
11. D. K. Lynch, "Step brightness changes of distant mountain ridges and their perception," Appl. Opt. **30,** 3508–3513 (1991).
12. S. D. Gedzelman, "Atmospheric optics in art," Appl. Opt. **30,** 3514–3522 (1991).
13. F. Cozman and E. Krotkov, "Depth from scattering," in *Proceedings of the IEEE Conference on Computer Vision and Pattern Recognition* (Institute of Electrical and Electronics Engineers, New York, 1997), pp. 801–806.
14. W. A. Shurcliff and S. S. Ballard, *Polarized Light* (Van Nostrand, Princeton, N.J., 1964), pp. 98–103.
15. G. P. Können, *Polarized Light in Nature* (Cambridge University, Cambridge, UK, 1985), pp. 1–10, 29–54, 60–62, 131–137, 144–145.
16. B. Cairns, B. E. Carlson, A. A. Lacis, and E. E. Russell, "An analysis of ground-based polarimetric sky radiance measurements," in *Polarization: Measurement, Analysis, and Remote Sensing*, D. H. Goldstein and R. A. Chipman, eds., Proc. SPIE **3121,** 382–393 (1997).
17. K. L. Coulson, "Polarization of light in the natural environment," in *Polarization Considerations for Optical Systems II*, R. A. Chipman, ed., Proc. SPIE **1166,** 2–10 (1989).
18. S. J. Hitzfelder, G. N. Plass, and G. W. Kattawar, "Radiation in the earth's atmosphere: its radiance, polarization, and ellipticity," Appl. Opt. **15,** 2489–2500 (1976).
19. D. K. Lynch and P. Schwartz, "Rainbows and fogbows," Appl. Opt. **30,** 3415–3420 (1991).
20. M. S. Quinby-Hunt, L. L. Erskine, and A. J. Hunt, "Polarized light scattering by aerosols in the marine atmospheric boundary layer," Appl. Opt. **36,** 5168–5184 (1997).
21. M. J. Raković, G. W. Kattawar, M. Mehrübeoğlu, B. D. Cameron, L. V. Wang, S. Rastegar, and G. L. Coté, "Light backscattering polarization patterns from turbid media: theory and experiment," Appl. Opt. **38,** 3399–3408 (1999).
22. D. B. Chenault and J. L. Pezzaniti, "Polarization imaging through scattering media," in *Polarization Analysis, Measurement, and Remote Sensing III*, D. B. Chenault, M. J. Guggin, W. G. Egan, and D. H. Goldstein, eds., Proc. SPIE **4133,** 124–133 (2000).
23. L. J. Denes, M. Gottlieb, B. Kaminsky, and P. Metes, "AOTF polarization difference imaging," in *27th AIPR Workshop: Advances in Computer-Assisted Recognition*, R. J. Mericsko, ed., Proc. SPIE **3584,** 106–115 (1998).
24. O. Emile, F. Bretenaker, and A. Le Floch, "Rotating polarization imaging in turbid media," Opt. Lett. **21,** 1706–1708 (1996).
25. X. Gan, S. P. Schilders, and Min Gu, "Image enhancement through turbid media under a microscope by use of polarization gating method," J. Opt. Soc. Am. A **16,** 2177–2184 (1999).
26. H. Horinaka, K. Hashimoto, K. Wada, T. Umeda, and Y. Cho, "Optical CT imaging in highly scattering media by extraction of photons preserving initial polarization," in *International Symposium on Polarization Analysis and Applications to Device Technology*, T. Yoshizawa and H. Yokota, eds., Proc. SPIE **2873,** 54–57 (1996).
27. M. P. Rowe, E. N. Pugh Jr., J. S. Tyo, and N. Engheta, "Polarization-difference imaging: a biologically inspired

technique for observation through scattering media," Opt. Lett. **20,** 608–610 (1995).
28. J. G. Walker, P. C. Y. Chang, and K. I. Hopcraft, "Visibility depth improvement in active polarization imaging in scattering media," Appl. Opt. **39,** 4933–4941 (2000).
29. Y. Y. Schechner, J. Shamir, and N. Kiryati, "Polarization and statistical analysis of scenes containing a semireflector," J. Opt. Soc. Am. A **17,** 276–284 (2000).
30. H. Farid and E. H. Adelson, "Separating reflections from images by use of independent component analysis," J. Opt. Soc. Am. A **16,** 2136–2145 (1999).
31. S. K. Nayar, X. S. Fang, and T. Boult, "Separation of reflection components using color and polarization," Int. J. Comput. Vision **21,** 163–186 (1997).
32. S. Rahmann and N. Canterakis, "Reconstruction of specular surfaces using polarization imaging," in *Proceedings of the IEEE Conference on Computer Vision and Pattern Recognition* (Institute of Electrical and Electronics Engineers, New York, 2001), Vol. 1, pp. 149–155.
33. M. Saito, Y. Sato, K. Ikeuchi, and H. Kashiwagi, "Measurement of surface orientations of transparent objects by use of polarization in highlight," J. Opt. Soc. Am. A **16,** 2286–2293 (1999).
34. L. B. Wolff, "Polarization vision: a new sensory approach to image understanding," Image Vision Comput. **15,** 81–93 (1997).
35. C. F. Bohren and A. B. Fraser, "At what altitude does the horizon cease to be visible?" Am. J. Phys. **54,** 222–227 (1986).
36. E. J. McCartney, *Optics of the Atmosphere: Scattering by Molecules and Particles* (Wiley, New York, 1976).
37. J. S. Tyo, M. P. Rowe, E. N. Pugh Jr., and N. Engheta, "Target detection in optically scattering media by polarization-difference imaging," Appl. Opt. **35,** 1855–1870 (1996).
38. R. L. Lee Jr., "Digital imaging of clear-sky polarization," Appl. Opt. **37,** 1465–1476 (1998).
39. E. Hecht, *Optics*, 3rd ed. (Addison-Wesley, New York, 1998), pp. 340–342.
40. S. Chandrasekhar, *Radiative Transfer* (Dover, New York, 1960), pp. 24–37, 280–284.
41. M. Ben-Ezra, "Segmentation with invisible keying signal," in *Proceedings of the IEEE Conference on Computer Vision and Pattern Recognition* (Institute of Electrical and Electronics Engineers, New York, 2000), Vol. 1, pp. 32–37.
42. T. Prosch, D. Hennings, and E. Raschke, "Video polarimetry: a new imaging technique in atmospheric science," Appl. Opt. **22,** 1360–1363 (1983).
43. A. M. Shutov, "Videopolarimeters," Sov. J. Opt. Technol. **60,** 295–301 (1993).
44. L. B. Wolff, "Polarization camera for computer vision with a beam splitter," J. Opt. Soc. Am. A **11,** 2935–2945 (1994).
45. A. S. Glassner, *Principles of Digital Image Synthesis* (Morgan Kaufmann, San Francisco, Calif., 1995), Appen. G.4.
46. R. L. Lee Jr., "Horizon brightness revisited: measurements and a model of clear-sky radiances," Appl. Opt. **33,** 4620–4628 (1994).
47. Y. Y. Schechner, S. G. Narasimhan, and S. K. Nayar, "Instant dehazing of images using polarization," in *Proceedings of the IEEE Conference on Computer Vision and Pattern Recognition* (Institute of Electrical and Electronics Engineers, New York, 2001), Vol. 1, pp. 325–332.
48. J. E. Solomon, "Polarization imaging," Appl. Opt. **20,** 1537–1544 (1981).
49. For the calculation of the path radiance integral, we assume κ to be distance invariant. This is because typically most of the light in the scene comes from the Sun and sky and thus does not change much along the line of sight. Moreover, we assume that multiple scattering (which effects the angular scattering distribution) is dominated by single scattering.